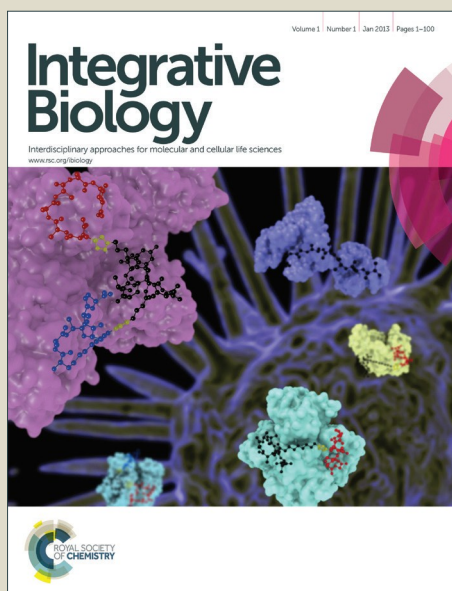


# Integrative Biology

Accepted Manuscript



This is an *Accepted Manuscript*, which has been through the Royal Society of Chemistry peer review process and has been accepted for publication.

*Accepted Manuscripts* are published online shortly after acceptance, before technical editing, formatting and proof reading. Using this free service, authors can make their results available to the community, in citable form, before we publish the edited article. We will replace this *Accepted Manuscript* with the edited and formatted *Advance Article* as soon as it is available.

You can find more information about *Accepted Manuscripts* in the [Information for Authors](#).

Please note that technical editing may introduce minor changes to the text and/or graphics, which may alter content. The journal's standard [Terms & Conditions](#) and the [Ethical guidelines](#) still apply. In no event shall the Royal Society of Chemistry be held responsible for any errors or omissions in this *Accepted Manuscript* or any consequences arising from the use of any information it contains.

**Insight:** The hybrid procedure described in the manuscript can predict, through analytic equations, experimental data concerning axonal outgrowth of neuron-like cells in a time range of 72 – 120 hours.

**Innovation:** This innovative computational/theoretical approach can model the behaviour of neuron-like cells on gratings, accounting for the twofold ability of topographical cues to simultaneously align and enhance the growth of cells

**Integration:** Thanks to the integration between advanced models and innovative fabrication techniques, the proposed approach will be useful to realize smart scaffold enabling axonal guidance during the neuronal regeneration.

# Deterministic control of mean alignment and elongation of neuron-like cells by grating geometry: a computational approach

Pier Nicola Sergi,<sup>\*a</sup> Attilio Marino,<sup>b,c</sup> and Gianni Ciofani<sup>c</sup>

Neuron-like cells are driven by their surrounding environment through local topography. A causal mechanotransductive web of topography-force relationships influences and controls complex cellular phenomena as growth and alignment. This work aimed at providing a computational framework able to model the behaviour of neuron-like (PC12) cells on gratings, accounting for the twofold ability of topographical cues to simultaneously align and enhance the growth of cells. In particular, starting from the mechanical behaviour of growth cone and filopodia, the effect of grating geometry (e.g., the periodicity and the size of grooves and ridges) on the neuritic mean alignment angle and on the outgrowth rate of cells was explored through theoretical tools and combinatorial simulations, which were able to predict ( $R^2 > 0.9$ ) experimental data in a time range of 72 – 120 hours.

## 1 Introduction

Living biological tissues are extraordinarily complex objects which have been investigated for a long time using approaches borrowed from biology and medicine. Nevertheless, they obey to the same physical laws and architectural principles which govern the non-living natural world<sup>1</sup>. Indeed, forces distributed among cells within multi-cellular tissues drive the morphogenic patterning, while cluster of cells modulate their rate of growth following internal stress patterns to allow each tissue to be shaped in a functional way. So, in general, form and mechanics are deeply entangled as well as structure and functions<sup>1,2</sup>. In particular, morphology, physiology and pathology of the nervous system were found to be considerably influenced by mechanics<sup>3</sup>, and complex phenomena as the growth of axons, the folding of the brain cortex and its compact wiring were discovered to be critically affected by mechanical interactions between neural cells and their biological environment<sup>4</sup>. Furthermore, morphogenesis of neural architectures is also entangled

<sup>a</sup> The Biorobotics Institute, Scuola Superiore SantAnna, Viale Rinaldo Piaggio 34, Pontedera, 56025 Italy. \* Corresponding author: Fax: +39 050 88 3101; Tel: +39 050 88 3059; E-mail: [p.sergi@sssup.it](mailto:p.sergi@sssup.it)

<sup>b</sup> The Biorobotics Institute, Scuola Superiore SantAnna, Viale Rinaldo Piaggio 34, Pontedera, 56025 Italy.

<sup>c</sup> Center for Micro-BioRobotics @SSSA, Istituto Italiano di Tecnologia, Viale Rinaldo Piaggio 34, Pontedera, 56025 Italy.

with topography in early developmental stages of the central nervous system, when "pioneers" axons act as natural scaffolds to align and guide other axons and neural cells<sup>5,6</sup>. Single neural cells are indeed driven by the local topography of their surrounding environment, which affects their internal signalling cascades and elicits morphological and functional changes. A causal mechanotransductive web of topography-force relationships influences and controls complex cellular phenomena as polarization, adhesion, proliferation, growth and alignment<sup>1,7-10</sup>. Moreover, the compliance of the underlying substrate is able to select between simultaneously growing neurons and astrocytes<sup>11</sup> (e.g., soft gels encouraged neurons and suppressed astrocytes), while its increase is also responsible for the enhancement (more than three times as much) of the branching ability of cells<sup>12</sup>. To approach this complex natural scenario, *in vitro* experiments were performed seeding neuron-like cells on flat surfaces and nanogratings to keep the main features of real biological phenomena with simplified boundary conditions. Indeed, from a side, neuron-like cells (PC12)<sup>13</sup> can reversibly adopt neuronal characteristics upon exposure to nerve growth factor and extend protrusions which are morphologically analogous to axons extending from primary sympathetic neurons<sup>14</sup>. From the other side, gratings have been used to mimic a natural three-dimensional extracellular matrix (ECM) thanks to their superficial alternation of ridge and groove lines<sup>15</sup>. Indeed, also during *in vitro* experiments, gratings were able to influence some important behaviours of neuron-like cells as polarization, adhesion, growth and alignment<sup>16-18</sup>, even if they were almost insensitive to stiffness changes for substrates stiffer than  $10^2$  Pa<sup>19</sup>. A similar behaviour was also described for murine neural progenitor cells (mNPCs)<sup>20</sup> and human mesenchymal stem cells (hMSC)<sup>21</sup>. In this case, the aspect ratio of gratings and the anisotropic substrate rigidity were found to influence the behaviour of cells, while an experimental correlation was described between hMSCs alignment and elongation. In particular, neuron-like cells (PC12) were able to indirectly sense physical cues (e.g. local topography and anisotropy of surfaces), through growth cone and filopodia<sup>22</sup>, which generally behave as biologic interfaces between the substrate and the inner of the cell. Since the material of substrate was much more stiff than growth cone and filopodia, while in general cellular traction forces were very low<sup>23</sup>, the magnitude of the stress/deformations fields was much more greater inside filopodia and growth cone<sup>24,25</sup>, because it was inversely proportional to the stiffness of materials. Therefore, a "mechanotransductive bridging mechanism" was involved in cells sensing of anisotropic rigidity and geometrical pattern, and both growth cone and filopodia were necessarily involved in this mechanism. Crucial questions are currently open on the nature of this kind of mechanism, and very little work has been done to investigate analytic equations able to predict cellular behaviours as alignment and elongation, starting from interactions between cellular transducer (e.g. filipodia and growth cone) and physical

characteristics of the substrates. Indeed, the alignment of PC12 neurites was found to be affected by ridge periodicity<sup>23</sup>, and their overall length experimentally appears to be related to the surface geometry, as in other cell models (e.g., hMSCs)<sup>21</sup>. Nevertheless, the role of the groove width still remains quite unclear, since no analytic expression was provided to predict its effect. As a consequence, this work theoretically and computationally investigated whether neuron-like cells were deterministically affected by both size and periodicity of grooves and ridges, and how explicit geometrical parameters (i.e., ridge width, ridge depth and groove width) influenced the alignment. Moreover, combinatorial simulations were used to predict how previous parameters influenced the overall length of PC12 neurites. Since analytic relationships are needed to implement reverse engineering of surfaces, these findings could be useful to implement the design of effective surfaces able to induce particular behaviours in cells. This knowledge could be synergistically used, together with experiments, in different scientific fields, as neuroengineering, to design effective regenerative interfaces<sup>26</sup>.

## 2 Materials and Methods

### 2.1 Experiments

PC12 neuron-like cells (ATCC CRL-1721) were plated on collagen-coated T-75 flasks and cultured in Dulbecco's modified Eagle medium (DMEM) supplemented with 5% fetal bovine serum (FBS), 10% horse serum (HS), 2 mM L-glutamine, 100 U/ml penicillin and 100  $\mu$ g/ml streptomycin. For differentiation induction, PC12 cells were plated on collagen-coated scaffolds and maintained for 3 days in DMEM supplemented with 1% FBS, 100 ng/ml NGF, 100 U/ml penicillin and 100  $\mu$ g/ml streptomycin. Scaffolds, constituted by aligned gratings, have been obtained through two-photon polymerization of the dedicated resistOrmocomp<sup>23</sup>. The immunostaining of vinculin was performed following standard immunocytochemistry procedures with a 1 : 50 dilution of the primary mouse IgG antibody (Millipore) followed by treatment with a 1 : 50 dilution of the secondary goat FITC-IgG anti-mouse (Millipore). Cytoskeletal f-actin and cell nucleus staining were performed by using TRITC-conjugated phalloidin (Sigma) and DAPI (Millipore), respectively. Fluorescence images were acquired with a confocal laser scanning microscope (C2s, Nikon). For the scanning electron microscope (SEM) imaging, samples fixed with 4% paraformaldehyde (PFA) were further treated with a 2.5% glutaraldehyde aqueous solution at 4°C for 30 min, followed by a progressive dehydration through an ethanol gradient (0%, 25%, 50%, 75% and 100% in de-ionized water). Samples were successively dried overnight and gold-sputtered before SEM investigation through an EVO MA10 (Zeiss). The measurement of the neurite length

was performed by using the Multi Measure plug-in of ImageJ software (<http://rsbweb.nih.gov/ij/>).

## 2.2 Connection among mean alignment, stiffness, deformation mode and geometry of gratings

The growth cone<sup>22,24</sup> regulates the outgrowth of both neural cells and neural like cells. The choice of the more suitable outgrowth direction is a complex task which also depends on the constraint distribution between growth cone and substrate<sup>27</sup>, as well as on the position of the tip adhesions under the adherent filopodia<sup>28</sup>. In this work, a novel approach<sup>25</sup>, accounting for both geometry and mechanics of growth cone and filopodia, was followed and further improved, as shown in Fig.1.

*Figure 1 about here*

The mean alignment of the current filopodium with respect to the main anisotropy direction of the grating was written as an explicit function  $\langle |\xi_g| \rangle: \mathfrak{R}^5 \supseteq Z \rightarrow \mathfrak{R}$ , where  $Z = G_w \times R_d \times R_w \times Y_0$ , and  $G_w, R_d, R_w$  were normalized geometrical parameters, while  $Y_0 = [E \times m_\varepsilon]$ ,  $E$  was the Young modulus of the surface (i.e. the nominal stiffness of grating),  $m_\varepsilon \in [\curvearrowright, \Rightarrow]$  was the mode deformation (i.e.  $\curvearrowright$ =bending,  $\Rightarrow$ =shear). More specifically, this quantity was written as:

$$\langle |\xi_g| \rangle = \frac{\pi}{4} - K\Psi(G_w, R_d, R_w) \quad (1)$$

where  $K$  was a function accounting for the influence of substrate stiffness and way of deformation,  $G_w = g_w \bar{g}_w^{-1}$  was the normalized groove width,  $R_d = r_d \bar{r}_d^{-1}$  was the normalized ridge depth,  $R_w = \langle R_{gc} \rangle r_w^{-1}$  was the normalized ridge width,  $g_w$  was the current groove width, while  $r_d$  and  $r_w$  were the current ridge depth and width, as shown in Figure 2(a).

*Figure 2 about here*

Similarly,  $\bar{g}_w, \bar{r}_d$  were normalization factors (i.e. given values of groove width and ridge depth, respectively  $\bar{g}_w = 33.45 \mu m$  and  $\bar{r}_d = 0.35 \mu m$ , taken from literature experiments<sup>18,23</sup>), and  $\langle R_{gc} \rangle \approx 1 \mu m$  was the mean radius of the non-spread PC 12 growth cone<sup>25</sup>. The function  $\Psi$  was expressed in a decoupled form as:

$$\Psi(G_w, R_d, R_w) = \prod_{i=G_w, R_d, R_w} \psi_i(i) \quad (2)$$

where each function  $\psi_i(i)$  depended on a single normalized parameter. In particular,  $K = \sum_j c_j K_j$  and the functions

$K_j : \Upsilon_0 \rightarrow \mathfrak{R}$ , with  $\Upsilon_0 = [E \times m_\varepsilon]$ ,  $j \in [b, s]$  ( $b$ =bending,  $s$ =shear) and  $c_j \in \mathfrak{R}$ , were used to account for the influence of the substrate stiffness coupled with the global effect of the dominant ways of deformation. Since for gratings the relevant deformations were mainly due to a combination of bending and shear<sup>21,29</sup>(as shown in Figure 2(b)),  $K$  was expressed as  $K = c_b K_b(E, \curvearrowright) + c_s K_s(E, \rightleftharpoons)$ , where  $K_b(E, \curvearrowright)$  and  $K_s(E, \rightleftharpoons)$  respectively considered the effects of bending and shear deformations. These two terms scaled differently with the geometry of grating (e.g. bending and shear deflections respectively were  $\delta_{bend} \propto (R_d/R_w)^3$ ,  $\delta_{shear} \propto (R_d/R_w)$ ), then the numeric values of  $K$  simultaneously resulted from both nominal stiffness and deformation modes coupled with geometric characteristics. In addition, according to literature references<sup>18,23</sup>, the overall value of  $K$  slightly increased with stiffness, as shown Figure 2(c). The function  $\psi_{G_w}(G_w) : \Upsilon_1 \rightarrow \mathfrak{R}$ , with  $\Upsilon_1 = [0, \infty[$ , was used to account for the influence of the groove width on the mean neuritic alignment. In particular, the flat surfaces corresponded to the cases  $G_w = 0$  and  $G_w \rightarrow \infty$ . In these cases, by definition, there was  $\psi_{G_w}(G_w) = 0$  and  $\psi_{G_w}(G_w) \rightarrow 0$ , and the Rolle's theorem predicted at least a point  $\zeta \in \Upsilon_1$  for which  $\psi'_{G_w}(\zeta) = 0$ . To account for the experimental course of the influence of the groove width in Eq. (2),  $\psi_{G_w}(G_w)$  was required to have only one maximum, which was furthermore bounded. Indeed,  $\langle |\xi_g| \rangle$  was positive and Eq. (2) led to  $\max(4\psi_{G_w}(G_w)) \leq \pi$ . Moreover, the condition  $\lim_{G_w \rightarrow \infty} \psi_{G_w}(G_w) = 0$  provided the lower bound of the function. As a consequence, not only  $\psi_{G_w}(G_w)$  was globally bounded, but also  $\psi'_{G_w}(G_w)$  was bounded, because  $\langle |\xi_g| \rangle$  globally ranged in the interval  $[0, \max(\psi_{G_w}(G_w))]$ . In general, then,  $\psi_{G_w}(G_w) \in C^{0,\alpha}(\Upsilon_1)$ , where  $0 < \alpha \leq 1$ ,  $C^{0,\alpha}(\Upsilon_1) = \{f \in C_b(\Upsilon_1) : [f]_\alpha < +\infty\}$  was the space of the  $\alpha$ -h lderian functions, and  $C_b(\Upsilon_1)$  was the class of the bounded and continuous functions over  $\Upsilon_1$ . Furthermore,  $[f]_\alpha$  was the  $\alpha$ -h lderian modulus of the function  $f$ , which was defined as follows:

$$[f]_\alpha = \sup_{x \neq y} \frac{|f(x) - f(y)|}{|x - y|^\alpha} \quad (3)$$

where  $x, y \in \Upsilon_1$ . In this work, for sake of simplicity,  $\alpha = 1$  and  $\psi_{G_w}(G_w) \in C^{0,1}(\Upsilon_1)$ . In other words,  $\psi_{G_w}$  was a Lipschitz function. As a consequence, the following relation holds:

$$\frac{|\psi_{G_w}(x) - \psi_{G_w}(y)|}{|x - y|} \leq M \quad (4)$$

where  $M \in \mathfrak{R}$  was the same for each  $G_w$  in the experimental range  $[x, y]$ . Therefore, the simplest function, which was able to approximate the course of the  $\psi_{G_w}(G_w)$  and satisfy both the previously listed boundary conditions for

$x < G_w < y$  ( $x > 0$  and  $y \ll +\infty$ ) together with Eq. (4), was  $\psi_{G_w}(G_w) = K_1(K_2 - G_w)$ , with  $K_1, K_2 \in \mathfrak{R}$ . The function  $\psi_{R_d}(R_d) : \Upsilon_2 \rightarrow \mathfrak{R}$ , with  $\Upsilon_2 = [0, q_q]$  and  $q_q \in \mathfrak{R}$ , was used to account for the influence of the ridge depth on the mean angle of alignment. The contacts between the growth cones and the grating mainly were on the ridges surfaces (at  $R_d = 0$ ) as well as the most of interactions. As a consequence, the influence of the ridge depth was assessed by using its Taylor expansion around  $R_d = 0$ :  $\psi_{R_d}(R_d) \simeq c + dR_d + O(R_d^2)$ . Considering that, by definition,  $\psi_{R_d}(0) = 0$  (flat surface), and neglecting the terms of a greater order,  $c = 0$  and  $\psi_{R_d}(R_d) \propto R_d$ . Finally, the function  $\psi_{R_w}(R_w) : \Upsilon_3 \rightarrow \mathfrak{R}$ , with  $\Upsilon_3 = [0, \infty[$ , accounted for the influence of the ridge width on the mean alignment angle. Geometrical and mechanical considerations, deriving from finite element (FE) models of growth cone and protruding filopodia<sup>25</sup>, led to express the mean alignment angle as a function of the positions, on the main ridge surface, of the emerging filopodia which had the maximum values of the Von Mises stress, as shown in Fig.1. For neural like cells (PC12), showing non-spread collapsed growth cones<sup>30</sup>, this procedure resulted in  $\psi_{R_w}(R_w) \propto \arctan(R_w)$ . As a consequence, Eq. (1) was rewritten as:

$$\langle |\xi_g| \rangle = \frac{\pi}{4} - [K_b(E, \curvearrowright) + K_s(E, \rightleftharpoons)] (A - G_w) R_d \arctan(R_w) \quad (5)$$

where  $A \in \mathfrak{R}$  was a numeric constant.

### 2.3 Combinatorial study of outgrowing axons

Combinatorial simulations of outgrowing axons were performed to quantitatively explore the axon like cells behaviour. Each developing neurite was modelled as a growing line adding segments along the time and the current position of the growth cone was written, through a finite difference system, as<sup>31–33</sup>:

$$\mathbf{p}(t+1) = \mathbf{p}(t) + \mathbf{l}(t+1) \quad (6)$$

where  $\mathbf{p}$  also coincided with the extremum of the neuritic path at the time  $t$ , while the current length of each segment was:

$$|\mathbf{l}(t+1)| = |\mathbf{l}(t)| [1 + \Omega(\langle |\xi_g| \rangle)] \quad (7)$$

where  $\Omega(\langle |\xi_g| \rangle)$  was the "enhancement function", accounting for the growth increase of the developing neurites. For each growth cone, and then for each neurite, the whole set of the most probable neuritic paths on the grating was computed. The growth cone, at each decisional step, was able to select one of the two most probable orientations due to the substrate characteristics and coming from Eq. (5). As a consequence, each growing segment had orientations  $\pm \langle |\xi_g| \rangle$  with respect to the main anisotropy direction, and for each growing step the sign was randomly chosen. Therefore, for a given set of conditions leading to a given mean alignment  $\langle |\xi_g| \rangle$ , the mean elongation of simulated neurites with respect to the neuritic length over flat substrates was defined as  $\langle \Lambda \rangle = \frac{\langle L_{grat} \rangle}{\langle L_{flat} \rangle}$  and written as:

$$\langle \Lambda \rangle = \sqrt{2} \left[ \frac{[1 + \Omega(\langle |\xi_g| \rangle)]^{M+1} - \Omega(\langle |\xi_g| \rangle) - 1}{[1 + \Omega(\pi/4)]^{M+1} - \Omega(\pi/4) - 1} \right] \frac{\Omega(\pi/4) \cos(\langle |\xi_g| \rangle)}{\Omega(\langle |\xi_g| \rangle)} \quad (8)$$

where  $M$  was the number of segments of each neurite.

*Figure 3 about here*

Finally, to test the reliability of computational methods, they were validated by crossing experimental data deriving from different experiments performed with neuron-like cells (PC12). In particular, novel data obtained from experiments presented in section 2.1 were used together with data from literature<sup>17,18,23</sup>.

### 3 Results

The PC12 neuron-like cells differentiated for 3 days on gratings were characterized by significantly longer neurites, and their alignment resulted substantially higher with respect to the control substrates. Moreover, a strong interaction between cells and structures could be appreciated, as reported in Fig.4. More specifically, Fig.4(a) depicts a confocal image reporting several points of contact, rich in vinculin expression, of PC12 cells with the Ormocomp gratings (in green: vinculin; in red: actin; in blue: nuclei). This intimate connection was finally confirmed by SEM imaging, as reported by Figs.4(b) and 4(c).

*Figure 4 about here*

In Fig.5(a), box plots of neuritic alignment were used to compare the alignment of PC12 neurites on different nanogratings and flat surfaces (A). When the groove width increased (B, C, D, that is the ridge distances were respectively equal to 2.5, 5 and 10  $\mu m$ ), the alignment values approached those on flat surfaces. However, a further effect of nanotopography was shown in quantile-quantile plots (Fig.5(b)), where the introduction of different kinds of nanograting

resulted in a change of form for the distribution of the neuritic alignments. To investigate the statistical meaning of the difference of alignment deriving from different substrates, the Wilcoxon rank sum test was performed several times. More specifically, this test resulted in  $p = 2.088 \cdot 10^{-8}$ , when substrates A and B were compared, while it resulted in  $p = 1.304 \cdot 10^{-8}$  and  $p = 8.095 \cdot 10^{-3}$  when B, C ( $G_w \simeq 0.06$  and  $G_w \simeq 0.13$ ) and C, D ( $G_w \simeq 0.13$  and  $G_w \simeq 0.28$ ) were respectively compared. Similarly, in Fig.5(c), the effects of patterns on neurites were shown: also in this case, the enhancement of growth lowered with the increase of the groove width, while the form of the distribution of lengths was kept among flat surfaces and gratings (see Fig.5(d)). The statistical significance of the difference of length between neurites, which were seeded on nanogratings and flat surfaces, was investigated. A Wilcoxon rank sum test resulted in  $p = 6.203 \cdot 10^{-4}$ , when the flat substrate was compared with B, while, when the B and C were compared, the same test resulted in  $p = 6.743 \cdot 10^{-5}$ . Finally, when the C and D substrates were compared, the test resulted in  $p = 0.1639$ . Furthermore, the flat substrate was separately compared with C and D leading respectively to  $p = 0.2635$  and  $p = 0.6827$ .

*Figure 5 about here*

The influence of the groove width was shown in Fig.6, where neuritic length values were plotted versus their alignment. The variation of this parameter was able to cluster different data sets. In particular, the effect of the groove width decreased when this parameter increased, and data deriving from surfaces with large groove width clustered similarly to those deriving from flat surfaces, even if some scattered data were due to biological variability.

*Figure 6 about here*

The influence of the grating geometry on the mean alignment of the neural like cells was modelled through Eq. (5), which had, in general, a three-dimensional domain  $Z$ . As a consequence, a reduction of  $Z$  dimensions was performed to allow a three-dimensional visualization of results. In Fig.7(a), the course of Eq. (5) was shown for a constant groove width ( $G_w = 1.5 \cdot 10^{-2}$ ) and variable ridge depth and width ( $R_d \in [0, 1]$  and  $R_w \in [0.5, 2]$ ). Similarly, in Figs.7(b) and 7(c), the course of the mean absolute alignment was shown respectively for  $R_d = 1$ ,  $G_w \in [0.05, 0.3]$ ,  $R_w \in [0.5, 2]$  and for  $R_w = 2$ ,  $G_w \in [0.05, 0.3]$ ,  $R_d \in [0, 1]$ . A further dimensionality reduction of  $Z$  was performed to compare theoretical predictions and experimental data. In particular, Eq. (5) with  $K = 0.290$  and  $A = 0.823$  was able to predict ( $R^2 \sim 0.99$ ) experimental values from<sup>17,18</sup>  $r_w = 0.350 \mu\text{m}$ ,  $g_w = 0.500 \mu\text{m}$ , and increasing values of the ridge depth (see Fig.7(d)). Similarly, in Fig.7(e), the course of the mean alignment was shown for increasing ridge grooves,  $r_w = 0.482 \mu\text{m}$  and  $r_d = 0.658 \mu\text{m}$ . In this case, Eq. (5) was able to predict experimental data<sup>23</sup> ( $R^2 \sim 0.99$ ) with  $K = 0.475$  and  $A = 0.823$ . Moreover, in Fig.7(f), similar performances were shown for  $g_w = 0.500 \mu\text{m}$  and  $r_d = 0.350 \mu\text{m}$ , and increasing val-

ues of the ridge width. Again, experimental data<sup>18</sup> were predicted ( $R^2 \sim 0.96$ ) with  $K = 0.850$  and  $A = 0.823$ .

*Figure 7 about here*

The course of combinatorial simulations was shown in Fig.8. More specifically, in Fig.8(a), the set of more probable paths of neurites was shown for a control flat surface (i.e.  $\langle |\xi_g| \rangle \approx \pi/4$ ). To investigate the main orientations of the whole set of trajectories, the Fast Fourier Transform (FFT) of the set of paths was performed and shown in Fig.8(b), where two main directions (i.e.  $\pm\pi/4$ ) were found. Moreover, in Fig.8(c) the density of neurites was explored through a profile plot, and paths clustered near the central axis. Similarly, the web of paths deriving from a further step of simulation on anisotropic surfaces (gratings) was shown in Fig.8(d), while the FFT of this web (Fig.8(e)) and its plot profile (Fig.8(f)) were plotted to show respectively the main orientations of the whole web of paths and the density of neuritic paths near the central axis. Finally, the complex web of paths for the final steps of simulations on gratings, the FFT of this web and the density profile near the central axis were respectively shown in Figs.8(g,h,i). In particular, the effect of the function  $\Omega(\langle |\xi_g| \rangle)$  on the length of the more aligned neurites was shown in Fig.8(g), as well as the nonlinear increasing of neuritic density close to the central axis (Fig.8(i)).

*Figure 8 about here*

Indeed, from a purely geometric point of view, the total length  $L$  was proportional to the mean angle of alignment (i.e.  $L \propto \cos(\langle |\xi_g| \rangle)$ , see Fig.3), and combinatorial simulations were used to explore whether just this geometrical effect was responsible to the enhancement of the neuritic length on gratings. As a consequence, first  $\Omega(\langle |\xi_g| \rangle) = 0$  and experimental normalized data were compared to the theoretical normalized elongation (i.e., the mean length on grating  $\langle L_{grat} \rangle$  ratio the mean length on the flat substrate  $\langle L_{flat} \rangle$ ). In Fig.9(a), it was shown that experimental results (see Figs.(4,5,6) obtained on gratings ( $E \simeq 1.27\text{GPa}$ ) and theoretical predictions diverged, further suggesting that  $\Omega(\langle |\xi_g| \rangle) > 0$ . In this work the following formulation was used for the "enhancement function"  $\Omega(\langle |\xi_g| \rangle)$ , that in its turn depended on  $G_w, R_d, R_w$  through Eq. (5):

$$\Omega(\langle |\xi_g| \rangle) = C_1 \left( \frac{100}{100 \langle |\xi_g| \rangle + 1} \right) \quad (9)$$

where  $C_1 \in \mathfrak{R}$ . Then, the course of the theoretical normalized neuritic length was shown in Fig.9(b) for  $C_1 = 2.5 \cdot 10^{-3}$ , and the mean curve (bold line) was now able to reproduce the experimental trend (see Figs.(4,5,6)), while experimental data were inside the upper and lower limits (standard deviations). Similarly, in Figs.9(c) and 9(d), data from literature experiments<sup>18,23</sup>(e.g. 4,5 days) were fitted as well. The

same function (with the same constants) was also able to reproduce different experimental data sets, which were obtained by using supports with comparable stiffness ( $E \simeq 2.47$  GPa and  $E \simeq 1.27$  GPa) with variable density of gratings. In simulations (see Fig.8), each growing neurite was modelled by using a chain of 10 elements, and to provide a meaningful statistics, 800 neurites were simulated for each angle of alignment.

*Figure 9 about here*

Finally, the performances of Eq. (8) were shown (Fig.10) in comparison to the computational data obtained through Eq. (6) and Eq. (7). The computational mean elongation of neurites was shown in function of the alignment (circles) and compared with the theoretical mean elongation, that was able to reproduce all the course of numeric data. The synergistic use of theory and experimental data (Fig.4(a),(b),(c)) allowed to analytically find the course of the mean elongation in function of both the mean alignment and time. In particular, this function was a generalized cylinder for  $\Xi(\langle |\xi_g| \rangle, \langle \Lambda \rangle, t) : \mathfrak{R}^3 \supseteq Q \rightarrow \mathfrak{R}$ , where  $Q = \langle |\xi_g| \rangle \times \langle \Lambda \rangle \times t$ , and  $t \in [72 - 120]$  hours, and it was expressed as:

$$\Gamma(\pi/4, M+1)\Omega(\langle |\xi_g| \rangle) \langle \Lambda \rangle - \sqrt{2}\Gamma(\langle |\xi_g| \rangle, M+1)\Omega(\pi/4)\cos(\langle |\xi_g| \rangle) = 0 \quad (10)$$

where  $\Gamma(\xi, M+1) = [1 + \Omega(\xi)]^{M+1} - \Omega(\xi) - 1$ , as shown in Fig. 10(b).

*Figure 10 about here*

## 4 Discussion

### 4.1 A biomimetic approach.

Neuron-like cells sense the external environment through the growth cone and filopodia, which are extremely specialized organs. They contemporarily belong to the cells and are in a tight contact with the surface over which the cells is growing. As a consequence, from a biological point of view, these organs can be seen as "frontiers", through which mechanotransductive stimuli have to flow. In other words, these organs are particularly involved in the complex process that allows the external physical (topographic) stimuli to be "correctly understood" by the cell. Therefore, in this work, both filopodia and growth cone, are accounted for as "doors" to explore how the cell can sense both external geometry and mechanical cues.

## 4.2 A shift of paradigm: from the surface to the growth cone

The mechanics and the geometry of surfaces are well known factors influencing the behaviour of cells, and both mechanical and geometrical characteristics of surfaces were directly used to infer and predict the behaviour of cells seeded and growing over engineered surfaces. On the contrary, a shift of paradigm is required when the starting points are growth cone and filopodia. Indeed, mechanics and geometry of external surfaces only indirectly influence the behaviour of cells through their sensing organs, and both geometry and mechanical characteristics of surfaces are perceived by the cells through the mechanics of growth cone and filopodia. As a consequence, their internal fields of stress and deformation were relevant to explore how the cell codes information due to geometry and stiffness and how it is able to translate external into internal information.

## 4.3 From biophysics to geometry

Neuron-like cells find the best neuritic path over a given substrate through a process which involves a complex interplay of random and deterministic factors<sup>34</sup>. Nevertheless, for each step of growth, the alignment of the leading filopodium depended on mechanical stress. Indeed, for each filopodium, the stress intensity scaled with the length, while it was independent on the alignment, so the local maximum stress on the boundary of the growth cone was at the intersection with the shortest stable filopodium. The cell (and locally the growth cone) tended to lower this local maximum, increasing the length of the shortest filopodium, which finally became the leading one, thus the neuritic growth was causally influenced by a stress-driven process<sup>25</sup>. An intriguing consequence is that the research of the most probable outgrowth direction was turned in the geometric research of the minimum length filopodium protruding from the growth cone. In other words, the mean solution of a complex biophysical problem was found through a geometric approach, which allowed the stochastic effects to be considered as superimposed to the deterministic solution.

## 4.4 Exploring the influence of the groove width

The previous process to find the most probable outgrowth direction of neuritic outgrowth was already shown to be simultaneously influenced by ridge width and depth (or by their combination)<sup>21</sup>. Nevertheless, the role of the groove width in the change of the mean angle of alignment still remained mysterious. As a consequence, the key role of this parameter in neuritic alignment was now expressed through Eq. (2). In this relationship,  $\psi_{R_d}(R_d)$  and  $\psi_{G_w}(G_w)$

were weighting factors, which accounted for the influences of ridge depth and groove width on the global interaction between growth cone and ridge, and, in particular,  $\psi_{G_w}(G_w)$  correctly accounted for the lowering of interactions when grooves increased their size. Furthermore, the flat surface was considered as a limit case for which temporarily  $g_w \rightarrow 0, r_d \rightarrow 0, r_w \rightarrow \infty$ , and Eq. (5) was able to predict a mean alignment of  $\pi/4$ , according to literature results<sup>16–18</sup>. In addition, Eq. (5) also modelled the coupled influence of stiffness and main deformation modes on the mean neuritic alignment. In general, local ridge deformations were complex and simultaneously due to tilt, dislocation, shear and bending<sup>29</sup>. Nevertheless, since grating stiffness was much more greater than cell stiffness, and traction forces were low<sup>23</sup>, tilt and dislocation were extremely low and negligible. Therefore, only shear and bending deformation were accounted for in Eq. (5). Moreover, the values of K function slightly increased together with stiffness (as shown in Fig. 2(c)), so alignment and elongation formally increased together with stiffness, according to literature results<sup>21</sup>. Nevertheless, the effect of stiffness (K function) was also coupled with geometric effects (functions  $\psi_{R_w}(R_w), \psi_{R_d}(R_d), \psi_{G_w}(G_w)$ ), which locally dominated interactions between gratings and cells within the experimental stiffness range (i.e., 1.27 – 2.47 GPa). As a consequence, the global effect of stiffness and geometry was practically the same for similar geometries within the previous stiffness range.

#### 4.5 Combinatorial simulations of outgrowing axons

The mean angle of alignment was a key factor for the neuritic building process. Indeed, the global neuritic outgrowth was locally led by the growth cone through a stress driven process able to select the leading filopodium, which, step by step, oriented the actual growing segment. This iterative process was then implemented through Eq. (6). Intriguingly, the only geometric increase of length, due to the progressive alignment of neurites, was not sufficient to explain the difference of length among substrates with different nanotopographical densities (Fig.9(a)). The further enhancement of growth was expressed through Eq. (8) and Eq. (9), which related the increase of the rate of growth to the mean angle of alignment through an increasing of the length of the adding segments. The same set of equations was able to reproduce the experimental behaviour of neural like cells on stiff substrates with different densities due to the alternate variation of both the groove width (at constant ridge width and depth)<sup>23</sup> and ridge width (at constant groove width and ridge depth)<sup>18</sup>. This effect was consistent with the biased formation of focal adhesions aligned to anisotropic superficial features (e.g. ridges, grooves)<sup>8,15</sup>. Indeed, these focal complexes were involved, through a signaling connection with cytoskeletal proteins, in an overall cellular response resulting in aligned and massive mor-

phological elongations<sup>8</sup>. The oriented outgrowth of neural like cells on gratings, showed then some similarities with morphogenetic processes, where different growth velocities were driven by a pattern of stress arising among clustered cells<sup>1,2</sup>. The external topographic pattern elicited an internal local stress pattern which governed the orientation of neurites, which through complex mechanotransductive processes, influenced their rate of growth. To model this complex behaviour, combinatorial simulations were used, to simulate all the more probable neuritic trajectories of a single outgrowing neurite. Since, for sake of simplicity, the more probable mean angles were chosen for each step of growth through Eq. (5) (see Fig.3(b)), the whole set of neuritic trajectories was inside the limit angle of  $2 < |\xi_g| >$ . As a consequence, for each neurite, the total length the mean path was  $L \propto \cos(< |\xi_g| >)$  (see Fig.3(a)), showing that a further "enhancement function" was necessary. Therefore, in silico simulations of outgrowing axons have been performed (see Fig.8) implementing a further growth of segments through Eq. (9). In other words, the more the neuritic segment was aligned, the more its outgrowth was "enhanced". This was in agreement with the greater stability of filopodia aligned on the grating<sup>20</sup>. Finally, the mean elongation of neurites was described through a generalized cylinder in the time range 72 – 120 hours. This implied that Eq. (8) was invariant in this time range, while the mean elongation was strongly dependent on the mean alignment.

## 5 Conclusion

The computational framework provided in this work was able to model the behaviour of neuron-like cells on gratings accounting for the two-fold ability of topographical cues to simultaneously align and enhance the growth of cells. The mean features of the real behaviour of neurites was modelled as a superimposition of deterministic and random factors and the mean deterministic solution of the coupled alignment-enhancement problem was found through a novel geometric approach expressed both in analytic formulas and computational algorithms. This framework could be used as a tool to explore the physiological behaviour of neural cells<sup>3,4</sup> as well as to improve the design of smart surfaces potentially involved in therapeutic strategies<sup>8,18,23</sup>. Similarly, it could be used to design neural circuits for advanced hybrid applications, and to rationalize the design of regenerative neural interfaces<sup>26</sup> by using topographical cues to control the regeneration of axons. Finally, this novel approach could be used together with models accounting for the internal activity of neural cell to better investigate the interactions between topographical and chemical cues on neural development and outgrowth<sup>35,36</sup>.

## 6 Figure captions

Figure 1 : Logic flow connecting experiments and analytic relationships through in silico models of growth cone and filopodia. Stress fields were obtained from Finite Element (FE) models accounting for both adhesion and traction of neuritic cytoskeleton. Therefore, they were used to obtain analytic relationships connecting grating geometry to the mean angle of alignment<sup>25</sup>. This approach, based of the mechanics of growth cone and filopodia, was used as starting point to implement original analytic relationships accounting for other physical cues (stiffness, deformation mode and density of grating) and implement new combinatorial simulation of neurites outgrowth.

Figure 2: (a) Relevant geometrical quantities of grating geometry:  $g_w$ : groove width;  $r_w$ : ridge width;  $r_d$ : ridge depth. (b) The local deformation of ridge, due to general cellular traction forces (i.e.,  $\mathbf{f}_{tot}$ ), was well approximated through a linear combination of two main modes of deformation: shear deformation, due to traction forces parallel to the ridge surface (i.e.,  $\mathbf{f}_1$ ); bending deformation, due to traction forces perpendicular to the surface (i.e.,  $\mathbf{f}_2$ ). (c) The numeric course of the K function is shown for increasing values of stiffness (i.e., 1.27 – 2.47 GPa), according to literature data<sup>18,23</sup>.

Figure 3: (a) Pictorial view of some possible neuritic paths on a directional anisotropic surface (grating). For each step of growth, all neurites accounted for the presence of the grating through the mean angle of alignment. For each cell all possible trajectories were made by segments with orientation  $\pm < |\xi_g| >$ , so they were within the limit angle of  $2 < |\xi_g| >$ . (b) Example of distribution of mean alignment angle for equilibrated segment chains with (i.e. equal frequency of - and + signs of the mean angle of alignment).

Figure 4: Adhesion and axonal guidance of PC12 neuron-like cells differentiated for 3 days on aligned gratings. (a) Confocal fluorescence acquisitions reporting PC12 focal adhesions (indicated by red rows), rich in vinculin expression, connected to theOrmocomp grating (in green: vinculin; in red: f-actin; in blue: nuclei). (b) SEM imaging of a single PC12 neural-like cell characterized by a well aligned neurite. (c) Growth cone of a neurite strongly interacting with theOrmocomp grating.

Figure 5: (a) Box plot of neuritic alignment on flat surface (A) in comparison with the alignment of neurites on different gratings with increasing groove width (B, C, D) (b) Quantiles-quantiles plot of alignment distributions on flat and on different gratings with increasing groove width. It could be noted that the form of distributions changed between flat and grooved surfaces, while it was kept among different gratings. (c) Box plot of neuritic length on flat surface (A) and on different gratings with increasing groove width (B, C, D) (d) Quantiles-quantiles plot of alignment

distributions on flat and on different gratings with increasing groove width. It could be noted that, in this case, the form of distributions was kept both among different gratings and for flat surfaces.

Figure 6: The groove width was able to influence both length and alignment of neurites. Indeed, only varying this parameter, clusters were formed among different data sets. In particular, flat surfaces and gratings with high groove width produced data which was similarly clustered on the alignment-length plane (see A and D substrates), while gratings with a smaller groove width were able to change the positions of data clusters on the plane (see D and B substrates). However, in all cases, some scattered points were still present.

Figure 7: (a) The course of the mean angle of alignment was shown for a groove width of  $G_w = 1.5 \cdot 10^{-2}$  and variable ridge depth and width:  $R_d \in [0, 1]$  and  $R_w \in [0.5, 2]$ . (b) The course of the mean absolute alignment was shown respectively for  $R_d = 1$ ,  $G_w \in [0.05, 0.3]$ ,  $R_w \in [0.5, 2]$  and (c) for  $R_w = 2$ ,  $G_w \in [0.05, 0.3]$ ,  $R_d \in [0, 1]$ . (d) The theoretical expression of the mean angle was able to predict ( $R^2 \sim 0.99$ ) experimental values from<sup>17,18</sup> for  $r_w = 0.350\mu m$ ,  $g_w = 0.500\mu m$ , and increasing values of the ridge depth. (e) The course of the mean alignment was shown for increasing ridge grooves,  $r_w = 0.482\mu m$ , and  $r_d = 0.658\mu m$ : Eq. (5) was able to predict experimental data from<sup>23</sup> ( $R^2 \sim 0.99$ ). (f) Similar performances were shown for  $g_w = 0.500\mu m$  and  $r_d = 0.350\mu m$ , and increasing values of the ridge width: experimental data<sup>18</sup> were again predicted ( $R^2 \sim 0.96$ ) with  $K = 0.850$  and  $A = 0.823$ .

Figure 8: (a) In silico combinatorial simulations of outgrowing axons: the set of the all neuritic paths was plotted for a flat substrate. (b) The Fast Fourier Transform (FFT) of the whole set of trajectories in (a) was plotted to investigate the main directions of the whole web: two main directions related to the limit angle were found. (c) The normalized density of segments was plotted versus their position with respect to the central axis, to explore the clustering of neurites. (d) Further steps of combinatorial simulations: these simulations accounted for the presence of gratings able to gradually increase the alignment of neurites. (e) FFT of the whole web of trajectories in (d) showing different and decreasing limit angles. (f) Plot of the normalized density of segments with respect to the position of the mean axis. (g) Final steps of combinatorial simulations: the enhancement of neuritic outgrowth was particularly clear for the more aligned neurites. (h) FFT of the whole set of path shown in (g) with the set of limit angles. (i) The clustering of segment near the mean axis was also affect by the enhancement function.

Figure 9: (a) The normalized neuritic elongation (i.e.,  $\langle L_{grat} \rangle = \text{mean length on gratings ratio } \langle L_{flat} \rangle = \text{mean length on the control flat substrate}$ ) was computed accounting for the geometric increasing due to the alignment phenomenon. This approach led to  $L \propto \cos(\langle |\xi_g| \rangle)$ , but a comparison with experiments suggested that the only

geometrical alignment was not able to predict the real increasing of length. (b) Data from experiments (3 days, see Figs. 4,5,6) were obtained with stiff substrates ( $E = 1.27$  GPa) and a variable groove width. The course of these data were predicted and the actual values were fitted by using Eq. (8) and Eq. (9). (c) Experimental data (4 days) on stiff substrates ( $E = 2.47$  GPa) with variable ridge width<sup>18</sup>, were again predicted and fitted by accounting for both geometric increasing and enhancement of length of the adding segments. (d) Experimental data (5 days), on a stiff substrates ( $E = 1.27$  GPa) with variable groove width<sup>23</sup> were as well predicted and fitted by accounting for the pure geometric increasing together with the enhancement of the adding segments length.

Figure 10: (a) The computational course of the mean neuritic elongation in function of the mean alignment was plotted and compared to the theoretical mean elongation to show its ability to fit computational data over the whole definition interval. (b) The theoretical course of the mean neuritic elongation was plotted in function of both the mean alignment and time (range 72 – 120 hours) through a generalized cylinder.

## Acknowledgements

The authors gratefully acknowledge Dr. Timo Betz (Institut Curie, Paris) for his critical reading of the manuscript and for his suggestions.

## Conflict of interest

None

## Authors contribution

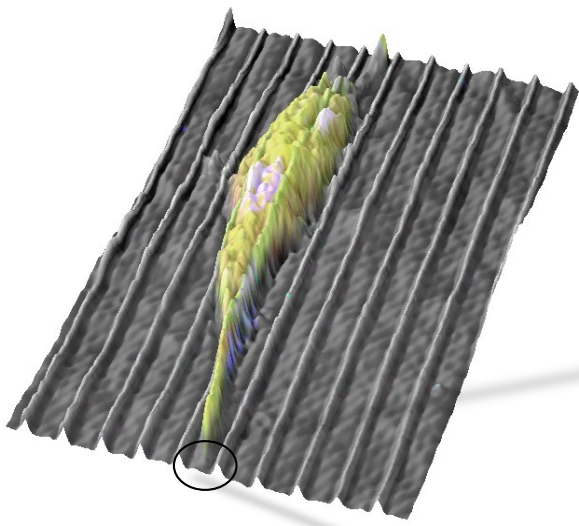
GC, AM conceived and performed experiments; PNS performed statistical analysis and conceived computational and theoretical approaches; GC, AM, PNS drafted the manuscript.

## References

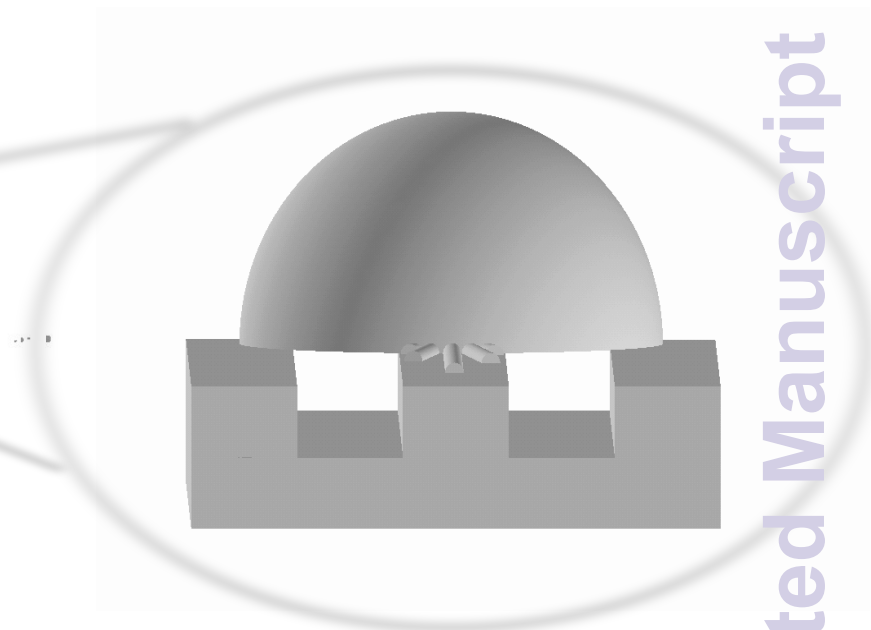
- 1 C. M. Nelson, R. P. Jean, J. L. Tan, W. F. Liu, N. J. Sniadecki, A. A. Spector and C. S. Chen, *Proceedings of the National Academy of Sciences of the United States of America*, 2005, **102**, 11594–11599.
- 2 D. E. Ingber, *Proceedings of the National Academy of Sciences of the United States of America*, 2005, **102**, 11571–11572.
- 3 K. Franze, *Development*, 2013, **140**, 3069–3077.

- 4 K. Franze and J. Guck, *Reports on Progress in Physics*, 2010, **73**, 094601.
- 5 S. Easter, L. Ross and A. Frankfurter, *The Journal of Neuroscience*, 1993, **13**, 285–299.
- 6 A. Chdotal and L. J. Richards, *Cold Spring Harbor Perspectives in Biology*, 2010, **2**, year.
- 7 N. Gomez, S. Chen and C. E. Schmidt, *Journal of The Royal Society Interface*, 2007, **4**, 223–233.
- 8 C. Bettinger, R. Langer and J. Borenstein, *Angewandte Chemie International Edition*, 2009, **48**, 5406–5415.
- 9 N. Arimura and K. Kaibuchi, *Nat Rev Neurosci*, 2007, **8**, 194–205.
- 10 S. Fujita, M. Ohshima and H. Iwata, *Journal of The Royal Society Interface*, 2009, **6**, S269–S277.
- 11 P. C. Georges, W. J. Miller, D. F. Meaney, E. S. Sawyer and P. A. Janmey, *Biophysical Journal*, **90**, 3012–3018.
- 12 L. A. Flanagan, Y.-E. Ju, B. Marg, M. Osterfield and P. A. Janmey, *NeuroReport*, 2002, **13**, –.
- 13 L. A. Greene and A. S. Tischler, *Proceedings of the National Academy of Sciences*, 1976, **73**, 2424–2428.
- 14 J. D. Foley, E. W. Grunwald, P. F. Nealey and C. J. Murphy, *Biomaterials*, 2005, **26**, 3639–3644.
- 15 K.-J. Jang, M. S. Kim, D. Feltrin, N. L. Jeon, K.-Y. Suh and O. Pertz, *PLoS ONE*, 2010, **5**, e15966.
- 16 A. Ferrari, M. Cecchini, M. Serresi, P. Faraci, D. Pisignano and F. Beltram, *Biomaterials*, 2010, **31**, 4682–4694.
- 17 A. Ferrari, P. Faraci, M. Cecchini and F. Beltram, *Biomaterials*, 2010, **31**, 2565–2573.
- 18 A. Ferrari, M. Cecchini, A. Dhawan, S. Micera, I. Tonazzini, R. Stabile, D. Pisignano and F. Beltram, *Nano Lett*, 2011, **11**, 505–511.
- 19 J. B. Leach, X. Q. Brown, J. G. Jacot, P. A. DiMilla and J. Y. Wong, *Journal of Neural Engineering*, 2007, **4**, 26.
- 20 J. S. Chua, C.-P. Chng, A. A. K. Moe, J. Y. Tann, E. L. Goh, K.-H. Chiam and E. K. Yim, *Biomaterials*, 2014, **35**, 7750 – 7761.
- 21 S. Wong, S.-K. Teo, S. Park, K.-H. Chiam and E. Yim, *Biomechanics and Modeling in Mechanobiology*, 2014, **13**, 27–39.
- 22 L. A. Lowery and D. V. Vactor, *Nat Rev Mol Cell Biol*, 2009, **10**, 332–343.
- 23 A. Marino, G. Ciofani, C. Filippeschi, M. Pellegrino, M. Pellegrini, P. Orsini, M. Pasqualetti, V. Mattoli and B. Mazzolai, *ACS Applied Materials and Interfaces*, 2013, **5**, 13012–13021.
- 24 T. Betz, D. Koch, Y.-B. Lu, K. Franze and J. A. Ks, *Proceedings of the National Academy of Sciences*, 2011, **108**, 13420–13425.
- 25 P. N. Sergi, I. Morana Roccasalvo, I. Tonazzini, M. Cecchini and S. Micera, *PLoS ONE* 8(8): e70304., 2013.
- 26 X. Navarro, T. B. Krueger, N. Lago, S. Micera, T. Stieglitz and P. Dario, *Journal of the Peripheral Nervous System*, 2005, **10**, 229–258.
- 27 C. Arregui, S. Carbonetto and L. McKerracher, *The Journal of Neuroscience*, 1994, **14**, 6967–6977.
- 28 M. B. Steketee and K. W. Tosney, *The Journal of Neuroscience*, 2002, **22**, 8071–8083.
- 29 I. Schoen, W. Hu, E. Klotzsch and V. Vogel, *Nano Letters*, 2010, **10**, 1823–1830.
- 30 A. Mingorance-Le Meur, A. N. Mohebiany and T. P. O'Connor, *PLoS ONE*, 2009, **4**, e4334.
- 31 R. Segev and E. Ben-Jacob, *Neural Networks*, 2000, **13**, 185 – 199.
- 32 R. Borisyuk, T. Cooke and A. Roberts, *Biosystems*, 2008, **93**, 101–114.
- 33 R. Borisyuk, A. K. a. Azad, D. Conte, A. Roberts and S. R. Soffe, *PLoS ONE*, 2014, **9**, e89461.
- 34 S. Maskery and T. Shinbrot, *Annual Review of Biomedical Engineering*, 2005, **7**, 187–221.
- 35 E. Forbes, A. Thompson, J. Yuan and G. Goodhill, *Neuron*, 2012, **74**, 490–503.

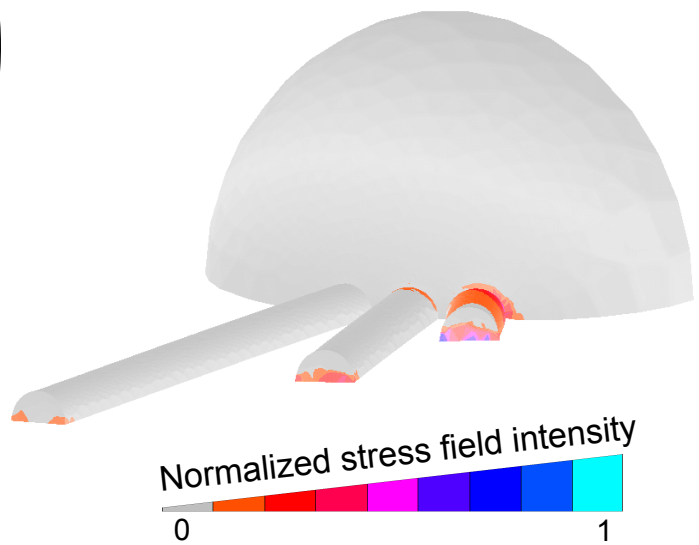
36 I. MoranaRoccasalvo, S. Micera and P. N. Sergi, *Scientific Report*, 2015, Accepted.



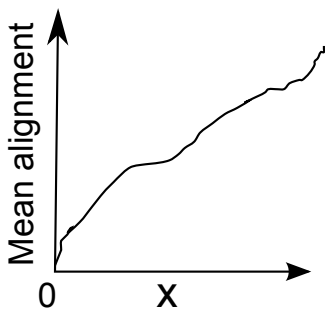
EXPERIMENTS



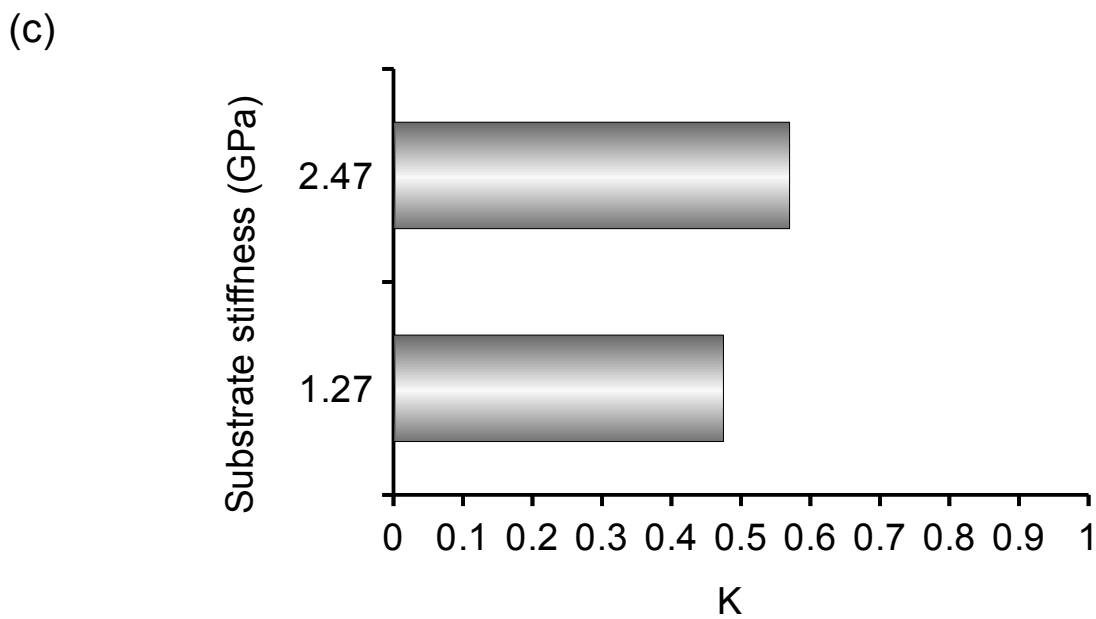
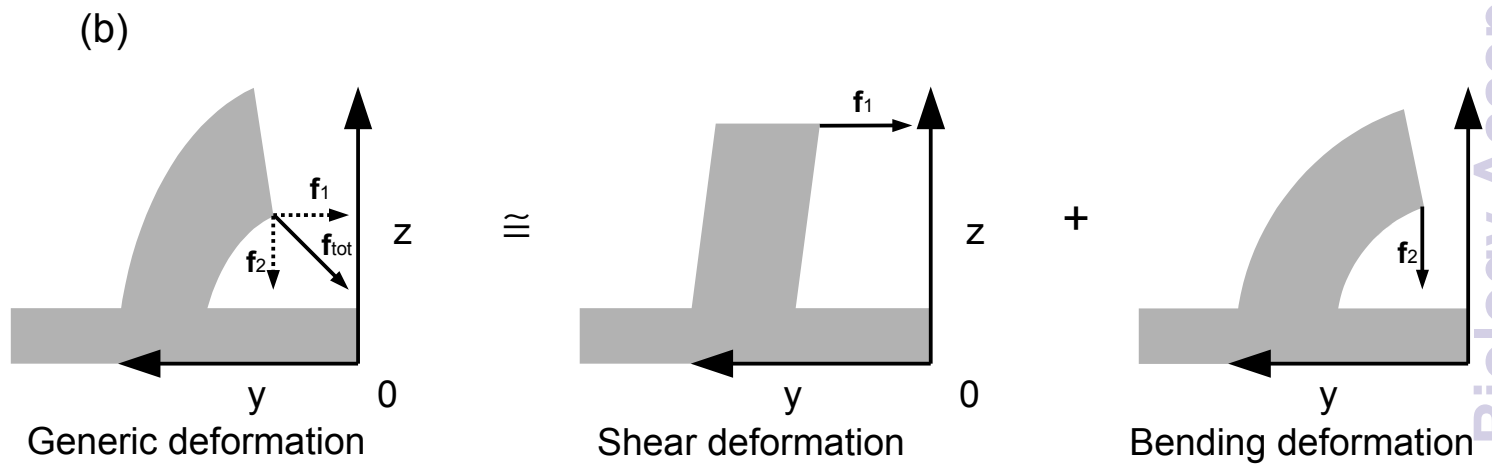
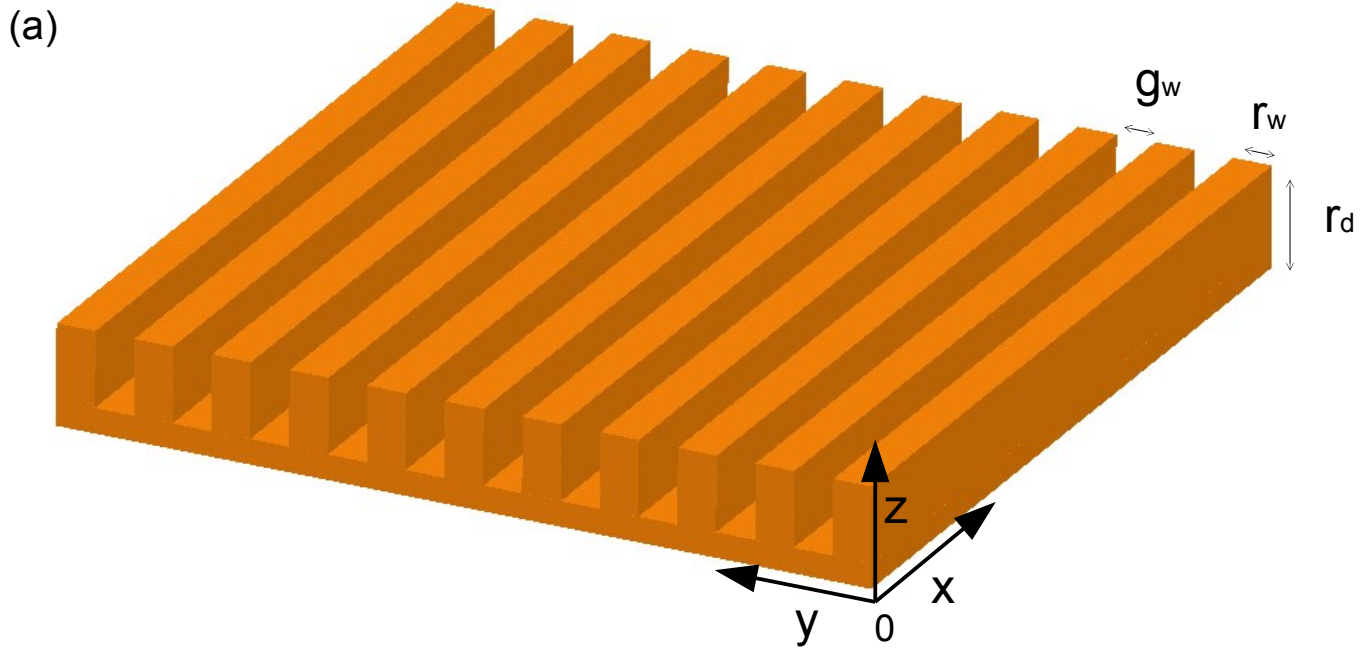
GEOMETRIC MODELS OF GRATINGS AND GROWTH CONE WITH FILOPODIA

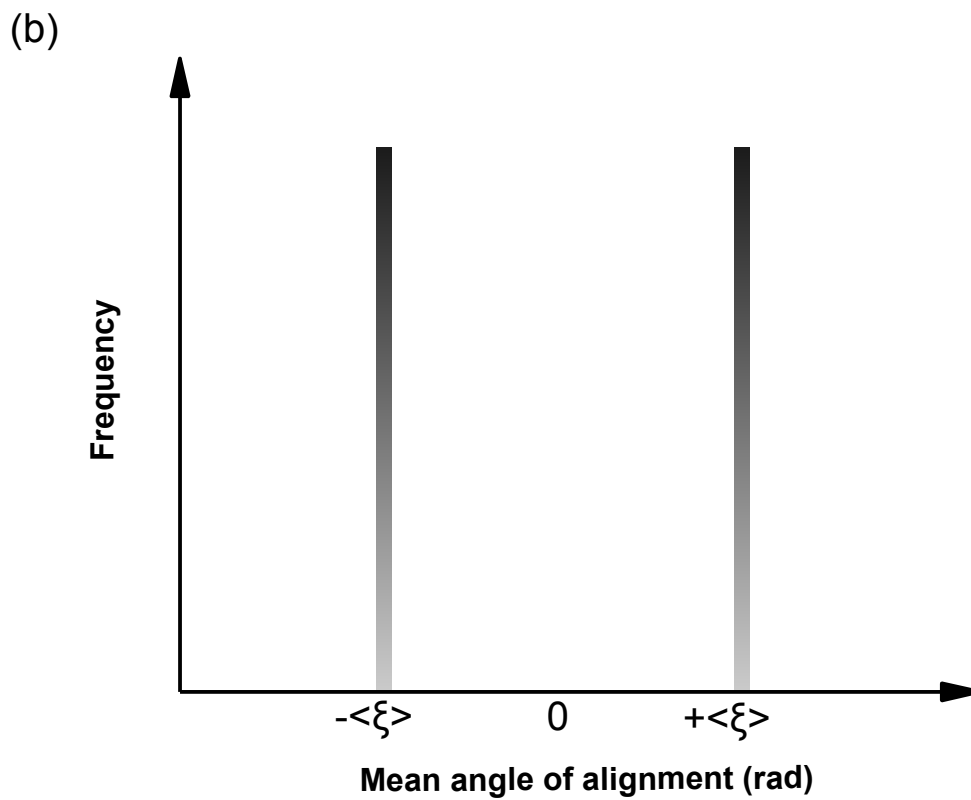
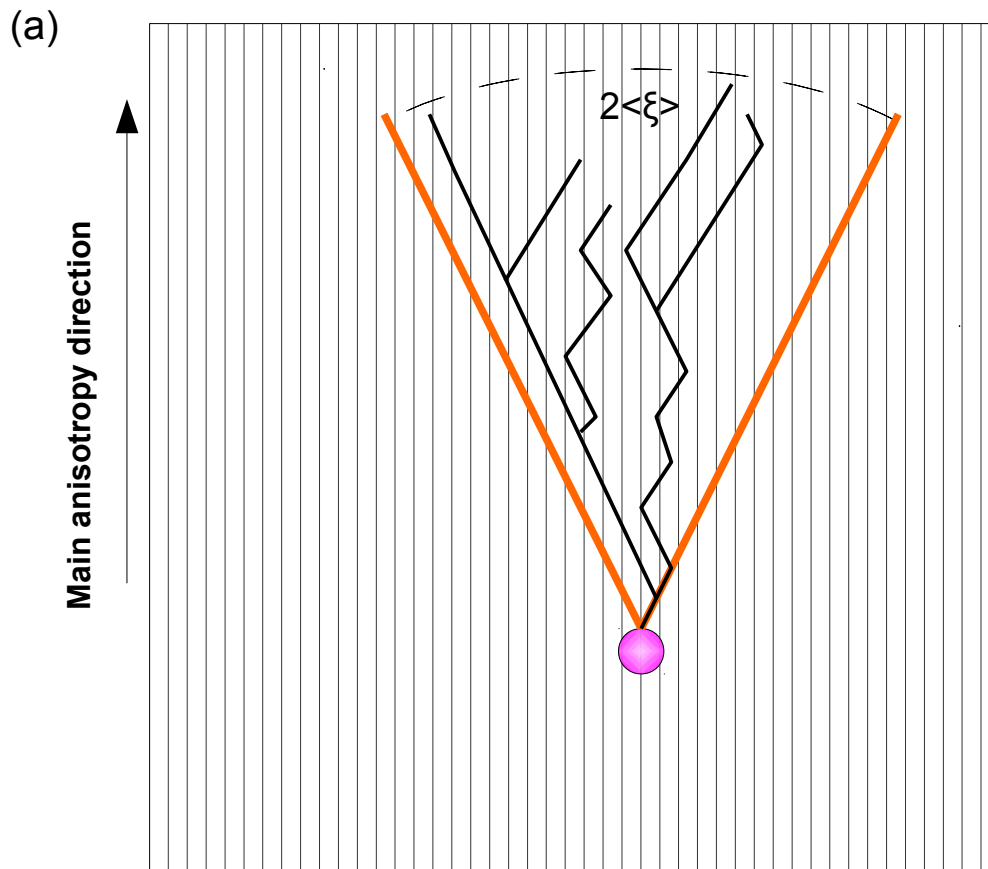


FINITE ELEMENT MODELS & INTERNAL FIELDS ANALYSIS OF GROWTH CONE AND FILOPODIA

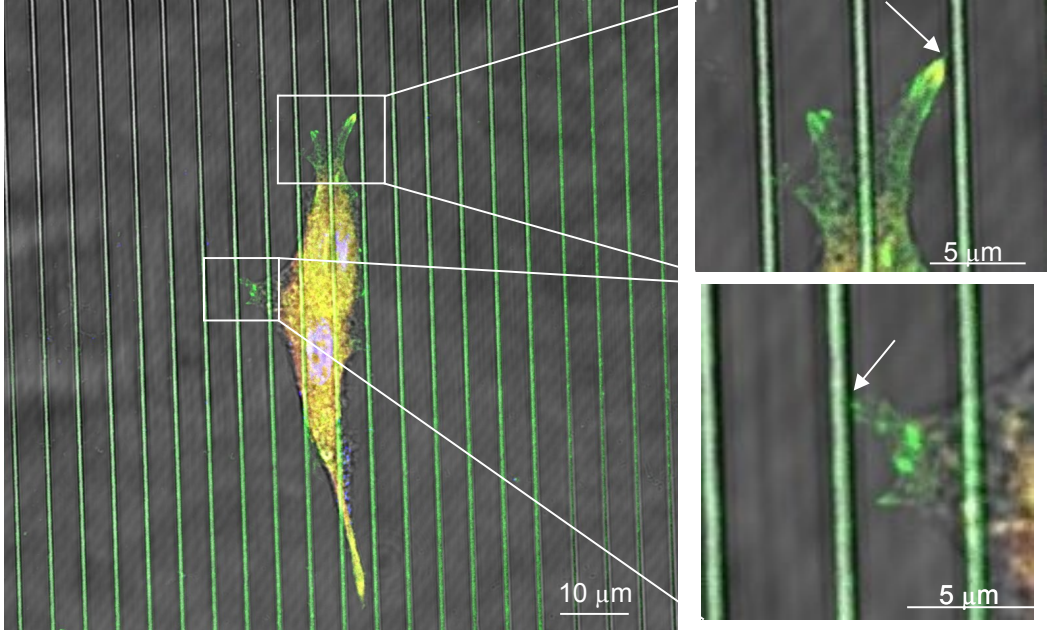


ANALYTICAL RELATIONSHIPS BETWEEN PHYSICAL CUES AND MEAN ALIGNMENT

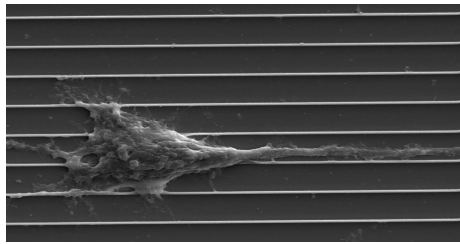




(a)



(b)



(c)

